Acquiring of photosensitivity by Mycobacterium tuberculosis in vitro and inside infected macrophages due to accumulation of endogenous Zn-porphyrins

Alexander Savitsky (apsavitsky@inbi.ras.ru)
Federal Research Centre ‘Fundamentals of Biotechnology’ of the Russian Academy of Sciences
Margarita Shleeva
Federal Research Centre ‘Fundamentals of Biotechnology’ of the Russian Academy of Sciences
Irina Linge
Central Tuberculosis Research Institute
Ivan Gligonov
Federal Research Centre 'Fundamentals of Biotechnology' of the Russian Academy of Sciences
Galina Vostroknutova
Federal Research Centre ‘Fundamentals of Biotechnology’ of the Russian Academy of Sciences
Denis Shashin
Federal Research Centre ‘Fundamentals of Biotechnology’ of the Russian Academy of Sciences
Andrey Tsedilin
Federal Research Centre ‘Fundamentals of Biotechnology’ of the Russian Academy of Sciences
Alexander Apt
Central Institute for Tuberculosis, Moscow, Russia TB-Stopper
Arseny Kaprelyants
Federal Research Centre ‘Fundamentals of Biotechnology’ of the Russian Academy of Sciences

Article

Keywords: Mycobacterium tuberculosis, porphyrin, photodynamic inactivation, dormant mycobacteria, 5-aminolaevulinic acid

Posted Date: October 3rd, 2023

DOI: https://doi.org/10.21203/rs.3.rs-3348857/v1

Additional Declarations: No competing interests reported.

Version of Record: A version of this preprint was published at Scientific Reports on January 8th, 2024. See the published version at https://doi.org/10.1038/s41598-024-51227-z.

Abstract

Mycobacterium tuberculosis (*Mtb*) is able to transition into a dormant state, causing the latent state of tuberculosis. Dormant mycobacteria acquire resistance to all known antibacterial drugs and can survive in the human body for decades before becoming active. In the dormant forms of *M. tuberculosis,* the synthesis of porphyrins and Zn-complexes significantly increased when 5-aminolevulinic acid (ALA) was added to the growth medium. Transcriptome analysis revealed a certain activation of genes involved in the metabolism of tetrapyrroles during the transition of *Mtb* into a dormant state, which may lead to the observed accumulation of free porphyrins. Dormant *Mtb* viability was reduced by more than 99.99% under illumination for 30 minutes (300 J/cm^2) with 565 nm light that correspond for Zn-porphyrin and coproporphyrin absorptions. We did not observe any PDI effect using active bacteria *in vitro*. However, after accumulation of active cells in lung macrophages and their persistence within macrophages for several days in the presence of ALA, a significant sensitivity of active *Mtb* cells (ca. 99.99%) to light exposure was developed. These findings create a perspective for the treatment of latent and multidrug-resistant tuberculosis by the eradication of the pathogen in order to prevent recurrence of this disease.

INTRODUCTION

Currently, antituberculosis treatment in the clinic faces significant problems due to spreading antibiotic-resistant strains of the pathogen. In addition to this genetically determined resistance, there is a resistance arising from physiological plasticity of mycobacteria. Thus, about one-quarter of the world's population has tuberculosis infection in the latent form, which is caused by the transition of the pathogen into a state of dormancy. Dormant cells of mycobacteria are characterized by low metabolic activity and the absence of syntheses of macromolecules and the cell wall. The known anti-tuberculosis drugs applicable in medical practice are not active against dormant mycobacteria. In recent years, it has been demonstrated that infection with COVID-19 often results in the transition of latent tuberculosis into an active form, which in a significant percentage of cases turns out to be drug-resistant[1]. This situation calls for a search for and development of new approaches designed to combat resistant forms of infection[2].

Antimicrobial photodynamic inactivation (aPDI) is one of the alternatives to the antibiotic approach that is able to inactivate bacteria, including antibiotic-resistant forms. Antibiotics and aPDI can act synergistically[3].

One of the most effective photosensitizers are porphyrins[4], among which zinc complexes standout[5–11]. Zn-coproporphyrin is considered as a promising compound for PDT of tumors[12].

The antimicrobial effect of aPDI by exogenic photosensitizers is limited by the ability of photosensitizers to interact with bacteria and penetrate through the highly organized outer membrane of microorganisms[13], especially mycobacteria.

More promising approach seems to be the usage of endogenous porphyrins, the synthesis of which can be stimulated by adding a precursor of heme synthesis, 5-aminolevulinic acid (ALA), to growing bacteria. ALA can penetrate into bacteria, for example, *Haemophilus parainfluenzae*, through hydrophilic pores present in membranes[14].

The observed accumulation of endogenous porphyrins during the transition of *Mycolicibacterium (basonym: Mycobacterium) smegmatis* cells into a dormant state[15] creates the prerequisites for possible aPDI of these bacterial forms. Indeed, we found that illumination of *M.smegmatis* cells led to the inactivation of dormant bacteria, in contrast to the effect of light on vegetative cells taken from logarithmic growth phase[16,17].

However, neither exploitation of endogenous PSs nor their ALA-mediated induction for aPDI has been studied in relation to *Mycobacterium tuberculosis (Mtb)*.

The aim of this work was to study the possibility of photoinactivation of vegetative and dormant forms of *Mtb* using endogenous porphyrins.

In this study, we report on significant accumulation of porphyrins and Zn porphyrins in *Mtb* cells after growth in the presence of ALA for vegetative and dormant states which results in very high sensitivity of bacteria in both physiological states to photoinactivation *in vitro* and *ex vivo* in macrophages.

RESULTS

1. ALA-mediated stimulation of porphyrin synthesis in dormant and vegetative cells of *M. tuberculosis*

Dormant forms of *Mtb* contained an elevated (ca. 6 times more) amount of porphyrins in comparison with vegetative cells (0.25 ± 0.05 ng porphyrins/mg wet cell weight in dormant forms versus 0.033 ± 0.01 ng porphyrins/mg wet cell weight in vegetative cells) (Figure 1).

In order to stimulate the formation of heme synthesis metabolites ALA was added to vegetative *Mtb* cultures and at the stage of transition to the dormant state. Under gradual environmental acidification[18] in the late stationary phase (40-60 days from the moment of inoculation), a significant number of dormant forms appeared both without and in the presence of 3 mM ALA in the growth medium (Figure S1). The appearance of dormant forms was monitored by the decrease in uracil incorporation in the culture, as well as the development of “non-culturability” (decrease in CFU number up to zero in contrast to high MPN number), as shown elsewhere[19,20] (Figure S1). The addition of ALA to the model system led to a more rapid development of the medium

The maximum production of porphyrins in vegetative *Mtb* cells in the presence of ALA was observed in 10 days after the addition of ALA to the culture, but the amount of porphyrins formed in vegetative *Mtb* was much less than in dormant mycobacteria (Figure 1).

An overall increase in the total amount of all porphyrins in dormant *Mtb* cells formed with ALA was 85 times up to a value of 17 ng/mg wet cell weight (Figure 1).

The pellet of bacteria grown in the presence of excess ALA differed significantly in color (reddish) from bacteria obtained without ALA (cream). For vegetative and dormant cells, this color was preserved in sediment after extraction with chloroform-methanol-water.

The absorption spectra of the chloroform-methanol extract of the vegetative *Mtb* cells grown in the presence of the ALA clearly indicated in the visible area the superposition of four-band spectra of the absorption of free (without metal) porphyrins (maxima 500, 540, 575 and 620 nm) and two-band spectrum characteristic of Zn-porphyrin (maxima at 545 and 575 nm) (Figure 2a). The difference between spectra of chlorophorm-methanol extract and spectra of pure coproporphyrin III in chlorophorm-methanol normalized to the absorbance at 500 nm practically coincides with the spectrum of pure Zn-coproporphyrin in the same solvent (Figure S3).

The fluorescence spectrum of the extract also corresponds to the fluorescence of the mixture of free porphyrin (maxima 620 and 685 nm) and Zn-porphyrin (the main maximum of 580 nm) (Figure 2a).

The absorption two-band spectra of the subsequent “Triton” extract mainly correspond to Zn-porphyrin (Figure 2b, S3).

An analysis of the fluorescence spectra of "Triton" extracts revealed that apart from the characteristic maxima at 620 and 680 nm typical for free porphyrins, there is an additional strong increase in the maximum at 580 nm typical for the Zn-porphyrin (Figure 2b, S3). The appearance of this maximum indicates that Triton X-100 preferably extracts Zn-coproporphyrin derivatives.

In the chloroform-methanol-water extract of dormant *Mtb* forms (grown without and with excess ALA), a low amount of porphyrins and Zn-porphyrins was detected. In the “Triton” extract absorption spectrum in the visible range, only a small fraction of four-band spectra typical of free porphyrin was observed, but pronounced two-band spectra of Zn-porphyrin derivatives were detected (Figure 2c). The examination of fluorescence spectra of the “Triton” extract of dormant *Mtb* cells grown in the presence of ALA revealed the presence of a signal characteristic of the Zn - porphyrin derivatives with maxima at 580, 620, and 680 nm (Figure 2c).

Since Zn-porphyrins have a pronounced phosphorescence and delayed fluorescence at room temperature[21], we carried out special measurements of “Triton” extracts in deoxygenated solutions (Figure 2c) to prevent quenching of the Zn-porphyrin triplet state. In a deoxygenated solution, the normalized spectrum showed the presence of a new peak at 710 nm (Figure 2c, S4b), characteristic of the triplet state. Since the measured lifetimes of phosphorescence at 710 nm (2.13 ms) and delayed fluorescence at 580 nm (2.25 ms) practically coincide (Figure S4d), type E delayed fluorescence (thermal activation from the triplet state to the singlet state)[22] evidently takes place (Figure S4d).

The fraction of Zn-porphyrins in the sample can be estimated based on the sum of all extracts determined spectrophotometrically in 0.1 N HCl using the extinction coefficients of porphyrin dication given in Falk's work[23]. The completeness of zinc dissociation in 0.1 N HCl was controlled spectrophotometrically by changing the position of the Soret band maximum. According to the absorption spectra of all the extracts (Figure 2), the total fraction of Zn porphyrins may reach 82% for dormant cells and 72% for active cells with ALA of the total amount of porphyrins (Figure 1).

An increase in the concentration of porphyrins for single-cell, both vegetative and dormant *Mtb* in the presence of ALA was confirmed by fluorescent confocal microscopy (Figure 3).

The fluorescence spectrum of single vegetative (Figure 3b) or dormant (Figure 3e) live cells of *Mtb* corresponds to the superposition of a large fraction of Zn-porphyrins' fluorescence and a small fraction of free porphyrins' fluorescence, similar to that described above (Figure 2).

The fluorescence lifetimes in a single mycobacterial cell (Figure 3c, f) are well described by a two-exponential decay with characteristic fluorescence life-times 1.81 ns for vegetative (Figure 3c) versus 1.76 ns for dormant (Figure 3f) for Zn-porphyrin and 12.6 ns versus 12.0 ns for free coproporphyrin that well correlate with the life-time 1.9 ns for Zn-coproporphyrin versus 14.81 ns for coproporphyrin in Triton X-100 (Figure S4c). Thus, single-cell measurements confirm intracellular localization of porphyrins and Zn-porphyrin derivatives in *Mtb* cells for both dormant and vegetative states.

Flow cytometry analysis also showed accumulation of the cell population with red fluorescence during transition to dormancy and long maintenance in this state (Figure S5). The percentage of fluorescent cells was 7% and 93% for 1 month's storage and 18 months' storage, respectively. In the presence of ALA, the percentage of fluorescent cells that contained porphyrins was substantially higher, reaching almost 100% for 18-month-old cells (Figure S5).

The obtained chloroform-methanol extracts of porphyrins were analyzed by LC-MS and HR-MS. According to LC-MS analysis of chloroform-methanol extracts of porphyrins in the dormant cells obtained in the presence of ALA, the concentration of uroporphyrin, coproporphyrin, and especially coproporphyrin tetramethyl ester increases in dormant *Mtb* cells (Table S1). In vegetative mycobacteria, ALA supplementation primarily stimulates uroporphyrin synthesis and a certain amount of coproporphyrin tetramethyl ester (Table S1). HR-MS analysis made it possible to reveal zinc-containing structures of porphyrins (Figure 4, Table S2).

Typical Zn isotope pattern[24] was found for Zn-porphyrins both for active and dormant *Mtb* cells. It was found that, unlike active *Mtb* cells, the unusual derivate of Zn-coproporphyrin, Zn-coproporphyrin tetramethyl ester, is present in dormant forms (Figure 4).

2. Transcriptomic analysis of cells of *M. tuberculosis* in a vegetative state and under transition into dormant state upon administration of exogenous ALA

In order to characterize possible biochemical changes in cells caused by ALA addition, a comparative transcriptomic analysis of active and dormant (early stage of transition to dormancy) *Mtb* cultures grown with and without the addition of ALA was carried out. Four variants of cultures were used for the analysis in three biological replicates each: (1) actively growing vegetative mycobacteria - 10 days of growth on a standard Sauton medium; (2) actively growing mycobacteria incubated for 2 hours with 3 mM ALA; (3) mycobacteria at an early stage of transition into a dormant state - 30 days; (4) mycobacteria at an early stage of transition to a dormant state incubated for 2 hours with 3 mM ALA. Comparative analysis of sequencing data was carried out in three groups: 1. active mycobacteria vs. dormant ones; 2. active mycobacteria vs. active mycobacteria to which ALA has been added; 3. dormant mycobacteria vs. dormant mycobacteria supplemented with ALA.

Changes in expression of 3929 of *M. tuberculosis* genes were analyzed.

A graphical analysis of the change in the ratio of the level of gene expression in comparison groups showed the following: dormant cells ~ active cells (act/dorm), active cells treated with ALA ~ active cells (ALA/act), cells upon transition to dormancy, treated with ALA ~ dormant cells (ALA/dorm) from the average normalized expression level, also show the maximum differences depending on the level of metabolic activity (transition to dormancy ~ metabolically active). Dormant cells show little response to ALA supplementation, as shown in Figure 5.

The transition into the dormant state led to an increase in the expression level of 153 genes ($p < 0.05$, FC > 2) and a decrease in the expression level of 157 genes calculated based on the comparison of normalized counts.

No genes involved in porphyrins metabolism were significantly (FC 2) impacted. However, as we stated elsewhere, transition into dormancy resulted in a substantial global decrease in mRNA content in *Mtb* cells[25], which makes it problematic to compare gene expression level in terms of their absolute quantities[26]. Therefore, we also performed differential expression analysis using a standard Z-statistical approach. The Z-standardization procedure reveals some enzymes of porphyrin metabolism, the expression level of which increases during the transition into the dormant state, as shown in Figure S6.

Thus, during the transition of *Mtb* cells into the dormant state, activation of genes associated with the metabolism of tetrapyrroles is observed, which can ultimately lead to the accumulation of free fluorescent tetrapyrrole compounds.

The addition of ALA to actively growing cells resulted in a statistically significant increase in the expression level of 9 genes and a decrease in the expression level of 81 genes based on a comparison of their transcript absolute quantities (Table S3). However, none of them belongs to porphyrin metabolism. This can be explained by the presence of a sufficient amount of intrinsic heme derivatives, which, according to the feedback principle, inhibit the initial steps of the biosynthetic pathway[27].

At the same time, visualization of the expression level, transformed on their Z-values, revealed ALA-dependent up-regulation of the following genes responsible for the metabolism of porphyrins: uroporphyrinogen-III synthase (Rv0260c, EC: 4.2.1.75) and uroporphyrin-III C-methyltransferase (Rv0511, EC: 4.2.1.75) (Figure S7) – SAM-dependent, membrane-bound methyltransferase methylating uroporphyrin III to form sirohydrochlorin [28].

Transcriptomic analysis also revealed an activation of the process of potassium ion transport into the vegetative cell due to the activation of Rv1030, Rv1031, an ATP-dependent potassium transport system (or Kdp) (Table S3) which catalyzes ATP hydrolysis in combination with electrogenic potassium transport into the cytoplasm[29]. In turn, it was shown that the activity of porphobilinogen synthase may be dependent on the presence of potassium ions[30].

The effect of ALA supplementation was also analyzed in relation to the gene expression level of a dormant culture of *Mtb*. Thus, there is a statistically significant increase in the expression level of the SAM-dependent methyltransferase Rv1405c (which was down-regulated upon transition into the dormant state), the function of which is not annotated (Table S3). Previously, increased expression of this gene has been observed *in vivo* in a mouse model of infection and has shown antigenic properties[31].

The assessment of the Z-normalized gene expression level plotted on the KEGG map makes it possible to detect an increase in the expression level of a number of genes of porphyrin metabolism (Figure S8). In particular, there is an increase in the expression level of the genes of the initial steps of heme biosynthesis: Rv0512 (porphobilinogen synthase EC: 4.2.1.24), Rv0510 (porphobilinogen deaminase/hydroxymethylbilane synthase, EC: 2.5.1.61), and Rv2677c (coproporphyrinogen III oxidase, EC: 1.3.3.4, EC: 1.3.3.15). This may contribute to the accumulation of coproporphyrin III in mycobacterial cells.

Thus, transcriptome analysis revealed a certain increase in the activity of a number of genes upon cell growth in the presence of ALA associated with the pathways of synthesis and metabolism of porphyrins and precorrins.

3. Photodynamic inactivation of *Mtb* cells

In order to elucidate how an increase in intracellular porphyrins concentration caused by the exogeneous addition of ALA influenced aPDI, active and dormant *Mtb* cells grown in the presence of ALA were exposed to LED light with a wavelength of 565 nm (power density 180 mW/cm^2), for 5-60 minutes.

As shown in Figure 6, illumination of suspension of active cells resulted in a slight decrease in viable cell concentration measured by MPN assay, while the same aPDI for dormant mycobacteria showed a more pronounced effect. Cells grown in the presence of ALA demonstrated very high sensitivity to illumination. In particular, dormant cells were sensitive, with 30 min of illumination resulting in >99.99% of bacterial killing.

Mycobacteria transition into dormancy under stressful conditions, including engulfment by lung macrophages during infection[32]. We assessed *in vitro* whether or not intracellular *Mtb* produce and accumulate porphyrins during 10-day persistence within purified lung macrophages and in the presence of ALA. As shown in Figure 7, these culture conditions led to the accumulation of porphyrins by captured bacteria. Remarkably, light sensitivity of mycobacteria captured by macrophages was significantly higher (almost complete sterilization) compared to that of bacilli multiplying in macrophage-free RPMI medium with ALA or conventional growth medium (Figure 8A). This difference was possibly due to an increased accumulation of porphyrins inside macrophages. To address this issue, we first incubated macrophages with ALA for 10 days and then added dormant mycobacteria for 16 hours before illumination. Visualization of macrophages incubated alone with ALA revealed the appearance of substances with fluorescence corresponding to that of porphyrins (Figure 8D). Moreover, dormant mycobacteria obtained in the presence of ALA were completely eliminated by light exposure if macrophages were pre-incubated with ALA (Figure 8B, C). Control dormant cells captured by such macrophages were also sensitive to PDI but to a lesser extent. These results suggest a synergistic effect of macrophages and ALA.

Photoinactivation was performed at 565 nm (300 J/cm^2). Viability of the mycobacteria was estimated by MPN assay. Bars represent (95%) confidence limits.

6. Influence of photodynamic inactivation on DCPIP reduction by *Mtb* cells

Because a significant amount of accumulated porphyrins in *Mtb* cells grown in the presence of ALA can be extracted with organic solvents/detergents, it is likely that these porphyrins are localized in cell membranes, as was found for *M.smegmatis*[15]. One of the significant membrane-linked processes is electron transport via respiratory chain. we measured DCPIP (dichlorophenolindophenol) reduction at the whole cell level. DCPIP, which is known as an acceptor of electrons, evidently interacted with a pool of reduced menaquinone[33]. Inactivation of menaquinone in isolated bacterial membranes of *M.luteus* results in the inhibition of respiratory chain activity[34]. Illumination of viable *Mtb* cells with an LED 565 nm produced no effect on DCPIP reduction rate. At the same time, cells grown in the presence of ALA showed a decrease in the DCPIP reduction rate up to zero after 15 min of illumination (Table 1). Due to negligible DCPIP reductase activity in dormant *Mtb* cells, such an experiment could not be performed for those cells.

Table 1. DCPIP reductase of *Mtb* cells change in DCPIP absorbance (600 nm) during first 20 min after start of the reaction. Averaged results of two independent biological replicates, each in three technical replicates, are shown.

FDI time(min)	Control (no ALA)	+ ALA
0	0,58±0.01	0,16±0.005
5	0,62±0.01	0,02±0.01
15	0,7±0.05	0
30	0,54±0.01	0
60	0,6±0.02	0

DISCUSSION

In the present study, we found elevated accumulation of porphyrins in dormant *Mtb* (Fig. 1); however, their concentration was low and evidently not enough for successful aPDI (Fig. 6). At the same time, adding ALA to growing *Mtb* before the transition to dormancy significantly increased the accumulation of porphyrins (Fig. 1).

Dormant cells of *Mtb* accumulated a significant amount of porphyrins extracted with organic solvents or by detergents, evidently indicating their possible membrane localization, as was established for *M.smegmatis*[15]. Such localization is likely due to the accumulation of unusual derivates of coproporphyrin - coproporphyrin tetramethyl ester according to LC-MS and HR-MS (Tables S1, S2; Fig. 4) along with copro- and uroporphyrins in cells grown with ALA. The genome of *Mtb* contains several genes coding for possible methyltransferases, which could be responsible for the identified modification of porphyrins.

The luminescence of Zn-porphyrin in microorganisms was described for the first time in[35], and later, it was also shown for *Mtb*[36]. Some Zn-porphyrins can be formed in mammalian organisms[37–39] including humans[40]. The biochemical role of Zn-porphyrins is still not fully understood. Zn-protoporphyrin is considered as a normal metabolite arising from iron deficiency during the development of anaemia, in particular, accompanying COVID-19[41]. At the same time, Zn-protoporphyrin is a competitive inhibitor of hemeoxygenase and regulates heme catabolism by controlling its conversion to bilirubin[42]. Zn-protoporphyrin fluorescence is also observed in human bronchial cancer and porphyries[39]. Zn-coproporphyrin is detected in parasites[21] and identified as growth factors released by *Sphingopyxis sp.*, enable laboratory cultivation of previously uncultured *Leucobacter sp.* through interspecies mutualis[43].

A biochemical role of Zn-coproporphyrin in mycobacteria may be associated with the regulation of heme metabolism[42]. In *Mtb*, coproheme (Fe-coproporphyrin III) was first synthesised and can convert to the protoheme by hydrogen peroxide-dependent heme synthase (EC:1.3.98.5) (https://www.genome.jp/entry/mtu:Rv2676c, Figure S7)[44,45]. Since Zn-coproporphyrin III cannot bind hydrogen peroxide, it becomes a competitive inhibitor and completely blocks protoheme biosynthesis along this pathway. Such a reversible way of blocking protoheme biosynthesis is in good agreement with

the concept of the dormant state. The possible biochemical role of the Zn-coproporphyrin is also supported by the presence of significant Zn-porphyrin fluorescence bands in related bacteria *M.smegmatis* and *Corynebacterium jeikeium*[46].

In our transcriptomic studies, we found that some genes coded for enzymes involved in tetrapyrroles metabolism appeared up-regulated under transition to the dormancy, among which there are the important genes Rv0512 - (delta-aminolaevulinic acid dehydratase), Rv0510 (porphobilinogen deaminase), and Rv0260c (uroporphyrinogen-III synthase) (Figure S6). The accumulation of porphyrins may be due to an insufficient amount of ferrochelatase for the conversion of the coproporphyrins to the coproheme for the over-expressed amount of coproporphyrin. The up-regulation of genes involved in the porphyrin biosynthesis pathway and transport was also observed under oxygen and carbon limitation for *M.smegmatis*[47]. At the same time, it was reported that the amounts of four proteins involved in porphyrin biosynthesis were increased in *Mtb* cells under starvation conditions (HemC, CysG, HemZ, and Rv1314c)[48]. Perhaps the different response of enzymes involved in porphyrin biosynthesis in our study and in published results could be explained by a substantial difference in establishing non-replicative conditions in both cases.

At the same time, the presence of ALA in growth medium leads to the activation of two genes in the initial part of the porphyrin biosynthesis pathway (Figures S7, S8); however, the activity of two genes responsible for terminal conversion of coproporphyrin either did not change or down-regulated (hemY) protoporphyrin IX magnesium-chelatase (EC 6.6.1.1.) (Figures S7, S8). In this case, the incorporation of zinc into the porphyrin macrocycle can proceed non-enzymatically at a fairly high rate[49].

A block for further consumption of porphyrins could also be established due to a decrease in protein biosynthesis at dormancy and a lack of final protein acceptors of protoheme.

The addition of ALA to bacterial culture dramatically increases the sensitivity of viable *Mtb* cells to illumination at 565 nm, where both coproporphyrin and Zn-coproporphyrin absorb light (Fig. 2). The most significant factor in this case may be illumination at the Zn-porphyrin absorption wavelength. Zn-porphyrin has a long-lived triplet state, which is known to play a decisive role in photodynamic therapy of tumors[50]. This effect of ALA was preserved for vegetative and dormant bacteria captured by lung macrophages and even enhanced if macrophages were precultivated with ALA, revealing a synergetic effect (Fig. 8).

The application of aPDI for inactivation of pathogenic bacteria has acquired significant attention in recent years. In this regard, a variety of exogenous photosensitizers are most common in killing bacteria[51] including mycobacteria [4], among which substances of a porphyrin nature were applied. Thus, *Mtb* with multiple antibiotic resistance was inactivated by aPDI using exogenous radachlorin[52]. Exogenously added porphyrins as photosensitizers were successfully applied for inactivating *Mycobacterium fortutinum*[53], *M. bovis* BCG[54], *M. marinum*[55], and *M.smegmatis*[56] *in vitro* and *in vivo*. Porphyrins conjugated with cyclodextrin were effective for aPDI in relation to *Staphylococcus aureus*[5].

However, due to the known limitations of exogenous photosensitizers for aPDI *in vivo* (problems of specificity, delivery to bacteria, penetration through bacterial cell wall) prompted the use of endogenous photosensitizers like those ubiquitously present in living cells - porphyrins of different structures. Induction of porphyrin synthesis in cells by ALA is the most well- known approach in PDI for anticancer therapy[57,58]. Recently, this approach has been used to inactivate pathogenic bacteria such as *Str. oralis* on the surface of titanium implants[59], *Mycobacterium abscessus*, leading to skin infections, *in vitro*[60,61]. Successful application of ALA-PDI was demonstrated for the curing of non-tuberculosis infection and cancer in clinic[62–65].

However, in the above experiments, ALA-PDI resulted in a decrease in bacterial viability measured by CFU of not more than one order of magnitude, which is far from full sterilization. Highly effective ALA-PDI found in the present study for active and especially dormant *Mtb* (Fig. 6) could reflect peculiarities of metabolism of slow-growing mycobacteria in active and non-replicative states. In the last case, absence of polymer biosynthesis *de novo*[18] should preclude resynthesis of damaged enzymes, including those involved in defense against radicals and active forms of oxygen. Evidently, the harmful conditions developed inside of macrophages after bacterium capturing in addition to ALA-mediated accumulation of host porphyrins enhance sensitivity of bacterial cells to aPDI, as was found experimentally (Fig. 8). Almost full sterilization of *Mtb* cells captured by macrophages makes this approach potentially useful for further medical application as alveolar macrophages are the first-line responders against *Mtb*.

The possible targets of antibacterial PDI in bacterial cells are the subject of continuing discussion, although primary destructive generation of reactive oxygen species upon PDI is a commonly accepted process[51]. Among putative targets, lipids via their peroxidation, nucleic acids, and proteins are under consideration[51]. The negative effect of PDI on iron metabolism and development of ferroptosis has been demonstrated for *Mycobacterium abscesus*[60]. In this study, we found a prominent effect of ALA-PDI on the functioning of endogenous respiration of mycobacteria (Table 1). This effect could be caused by either a decrease in respiratory substrate flow or direct inhibition of the respiratory chain. The last suggestion is plausible because of membrane localization of significant amount of porphyrins induced by ALA. *Mtb* respiratory contains succinate dehydrogenase with a membrane–bound Fes cluster[66], which is known as a sensitive target for ROS [67] and therefore for PDI. In addition, indirectly, PDI inducing modification of membrane lipid matrix[68] could influence respiratory chain activity. However, to make a final conclusion on the involvement of respiratory chain in the identified effect needs additional study with isolated mycobacterial membranes.

Thus, for the first time, we demonstrated the successful application of aPDI for the inactivation of *Mtb* cells *in vitro* and in macrophages due to a significant accumulation of endogenous porphyrins in the presence of 5-aminolevulinic acid.

In conclusion, the findings of this study provide a new perspective for the eradication of vegetative, including multidrug-resistant, and dormant forms of *Mtb* using endogenous porphyrins as

photosensitizers. It is logical to apply this approach first for TB with surface localization. However, using current progress in clinical development of photodynamic therapy of cancer[69], especially different light illumination techniques, including interstitial PDT, and endoscopic technic, localized TB focuses including those in the lungs and other organs could also be tackled by PDI.

MATERIALS AND METHODS

Formation of the dormant forms of M. tuberculosis upon the medium self-acidification

Inoculum was initially grown from frozen stock stored at − 70°C in 40% glycerol. To obtain dormant forms, we used the model of environmental acidification [18,70]. *Mtb* strain H37Rv was grown for 8 days (up to OD600 = 2.0) in Middlebrook 7H9 liquid medium (Himedia, India) supplemented with 0.05% Tween 80 and 10% growth supplement ADC (albumin, dextrose, catalase) (Himedia, India). Next, 1 ml of the initial culture was added to 200 ml of modified Sauton medium that contained (per liter) the following: KH_2PO4, 0.5 g; $MgSO_4$•$7H_2O$, 1.4 g; L-asparagine, 4 g; glycerol, 2 ml; ferric ammonium citrate, 0.05 g; citric acid, 2 g; 1% $ZnSO_4.7H_2O$, 0.1 ml; pH 6.0–6.2 (adjusted with 1 M NaOH) and supplemented with 0.5% BSA (Cohn Analog, Sigma), 0.025% tyloxapol and 5% glucose. Cultures were incubated in 500 ml flasks that contained 200 ml modified Sauton medium at 37°C with shaking at 200 rpm (Innova, New Branswick, NJ, USA) for 30–50 days, and pH values were periodically measured. In log phase, pH of the culture reached 7.5–8 and then decreased in stationary phase. When the medium in post-stationary phase *Mtb* cultures reached pH 6.0–6.2 (after 30–45 d of incubation for different experiments), cultures (50 ml) were transferred to 50 ml plastic tightened capped tubes and kept under static conditions, without agitation, at room temperature. At the time of transfer 2-(N-morpholino) ethanesulfonic acid (MES) was added in a final concentration of 100 mM to dormant cell cultures to prevent fast acidification of the spent medium during long-term storage. To induce the synthesis of porphyrins, 3 mM 5-aminolevulinic acid (ALA) was added to the cultures during the transition of mycobacteria into a dormant state (20 days after inoculation).

For the vegetative state, *Mtb* cells were cultivated in Middlebrook medium (Himedia, India) supplemented by ADC (Himedia, India) and 0.05% of Tween-80 with the addition of 3 mM 5-aminolevulinic acid. Cultures were cultivated for 14–30 days.

Extraction of porphyrins

The porphyrins were extracted from the biomass according to Bligh[71]. Bacteria were washed three times with 50 mM phosphate buffer (pH 7.4). Then, 1 ml of chloroform and 2 ml of methanol were added to the wet biomass of the cells (0.8 g). Cells were agitated for 12 h in the extraction mixture with subsequent centrifugation (4000 g, 20 min). The next extraction was performed during 12 h using 2% Triton X-100 in 20 mM Tris HCl buffer at pH 7.4.

For high-resolution mass spectrometry (HRMS), the porphyrins were extracted from dormant and vegetative mycobacteria 0.8 g the wet biomass of the cells using 3 ml of 75% acetone, 15% methanol with 10% water, or 3 ml of chloroform:methanol:water (1:2:0.8)[71].

Spectrophotometric, fluorescence, and phosphorescence analysis of porphyrin in mycobacterial extracts

The absorption spectra of the extracts were recorded in a 1 cm cuvette on a spectrophotometer Cary-50. Excitation and fluorescence spectra were recorded in a 3 mm cuvette on a Cary Eclipse spectrofluorometer in both fluorescence and phosphorescence modes at room temperature. To record the phosphorescence spectra, the extracts were mixed in a ratio of 1/10 with a deoxygenating solution containing sodium bisulfite (40 mg/ml $NaHSO_3$, 2% Triton X-100, pH 7.8) as described in [72]. Phosphorescence lifetimes were recorded in the same deoxygenating solution on a Cary Eclipse spectrofluorometer using the Lifetime program.

LC-MS

Porphyrin identification in chloroform-methanol extracts was carried out by LC-MS on an Agilent 1290 Infinity chromatograph (USA) with an Agilent 6460 TQ mass spectrometer (USA).

An Agilent Eclipse Plus C18 1.8 um 2.1x50 mm column was used with mobile phase: A – 0.1% formic acid in water, B – 0.1% formic acid in acetonitrile; Gradient A–B; column temperature – 40 ^{0}C, flow rate – 0.4 ml/min, detection – UV/VIS 400 nm, MS ESI(+) full scan. The mass spectra were acquired with positive electrospray ionization (ESI) with the ion spray voltage set at 5.5 kV. We used 1 µg of the porphyrin standards for the initial tests. Coproporphyrin III, uroporphyrin III and coproporphyrin III tetramethyl ester (BenchChem, USA) were used as standards. Due to the use of 0.1% formic acid in this type of LC-MS analysis, separate data on Zn-porphyrins were lost[42] and included in the total amount as free porphyrins.

High-Resolution Mass Spectrometry (HR-MS)

The presence of Zn-porphyrins was confirmed by HR-MS. HR-MS analysis of extracts was performed on an Impact II QqTOF high-resolution mass-spectrometer (Bruker Daltonik, Germany) equipped with Apollo II ESI ion source (Bruker Daltonik, Germany) under the following conditions: direct sample infusion at 30 µL/min, HV capillary at 4.5 kV for positive mode and 3.0 kV for negative mode, spray gas – nitrogen at 0.9 bar, dry gas – nitrogen at 4.0 L/min 200°C, scan range m/z 50-1200, 0.2 Hz scan rate, automatic internal calibration with sodium trifluoroacetate solution. Spectra were processed with Compass DataAnalysis 5.1 (Bruker Daltonik, Germany).

Confocal fluorescence microscopy, life-time measurements, and microspectrofluorimetry

Sample preparations: A volume of 2 ml of 10^9 *Mtb* cells was centrifuged at (8 000 rpm for 10 min); the bacterial pellet was washed with water twice and then resuspended in distilled 5 ml of water. After that, the suspension was applied to a glass cover slip and left to dry for a few minutes, then fixated with Merckoglass (Merck). After solidification of the Merckoglass, samples were used for microscopy.

Fluorescence lifetime measurements were performed on a PicoQuant MicroTime 200 confocal scanning system (Pico-Quant GmbH, Berlin, Germany) based on an Olympus IX-71 inverted fluorescence microscope (Japan). A high numerical aperture apochromatic objective (UApo N 100X, NA 1.49, oil immersed, Olympus) was used for excitation at 405 nm by an LDH-P-C-400B laser (Pico-Quant GmbH, Berlin, Germany) and emission was recorded using a 550 nm Longpass filter with an avalanche photodiode (SPAD, Perkin Elmer) using the TCSPC mode with a PicoHarp 300 board. SymphoTime® software was used for data collection. Original data obtained via microscope were recalculated to form FLIM images. In order to extract precise estimates of fluorescence lifetimes, histograms of pixels that belonged to cell areas were summing. The resulting histogram was then fitted with a biexponential decay model. The weighted least-squares approach was applied due to the heteroscedasticity largely presented in the data[73]. The BFGS (Broyden-Fletcher-Goldfarb-Shanno) algorithm was used for optimization because of its better performance in problems with large variation in data[74].

In order to prove the presence of porphyrins, single cell microspectrofluorimetry was used. Fluorescence spectra were recorded in the confocal mode of the MicroTime 200 system using a Shamrock 163 spectrograph with a Newton DU-970 camera (Andor, UK). Long-pass 550LP filter was used. Spectrographs were calibrated using reflection of the laser beam from a glass cover slip. Background subtraction of the single-cell fluorescence spectra was carried out according to the algorithm [75]. Obtained fluorescence spectra were smoothed with a Savitzky–Golay filter. Data analysis was performed using the MicroCal Origin 8.5 Pro software and Python 3.10.9 with additional packages for data analysis such as Numpy 1.22.2, SciPy 1.8.0, and Symfit 0.5.5. Matplotlib 3.5.1 package was used for data visualization.

For porphyrin visualization within the lung macrophages and engulfed mycobacteria cells were cultivated on coverslips in the presence of mycobacteria, as described below. At indicated time points, cells were fixed with 1% PFA for 10 minutes, washed with x1 PBS and stained with ActinGreen-488 (MolecularProbes by LifeTechnologies) and DAPI. Photography was performed under microscope AxioSkop40 (Zeiss, Germany), magnification x40. Macrophages, incubated alone with ALA, were procured for visualization directly in plate for cultivation. Photography was performed under inverted fluorescent microscope Axio Observer.A1 (Zeiss, Germany), AxioCam MRc5, filter for porphyrins: BP 546/12 – FT 580 – LP 590. Source data is available on the website https://doi.org/10.5281/zenodo.8322146

Flow cytometry analysis and microscopy

The *Mtb* cells were fixed by 2% formaldehyde for 24 h. Aliquots of bacterial samples—500 µl (OD600 ~ 0.2) were placed into the flow-cytometry plastic tubes. The CytoFlexS system (Beckman Coulter, USA) was used to measure porphyrin fluorescence of the bacterial cells.

The graphs were analyzed in coordinates FSC-A vs FL3-A (forward scattering vs. red fluorescence); the voltage on the detectors: FSC-A-10, FL3-A- 50. In total, 10,000 events were acquired at an analysis rate of 1000 events. Data analysis was carried out using the CytExpert software for the CytoFlex platform.

Phase-contrast and epifluorescence microscopy was carried out using a Nikon eclipse Ni-U microscope. Fluorescence microscopy was carried out in the FITC channel (EX = 465–495, DM = 505, BA = 515–555). Magnification×1500. Photos were taken using a Nikon DSQi2 camera (Japan). Analysis of the morphological changes was performed using the NIS-Elements BR software.

Isolation of lung macrophages

Mice of inbred strain C57BL/6JCit (B6) were bred and maintained under conventional conditions at the Animal Facilities of the Central Tuberculosis Research Institute (CTRI, Moscow, Russia) in accordance with guidelines from the Russian Ministry of Health # 755, and under the NIH Office of Laboratory Animal Welfare (OLAW) Assurance #A5502-11. Water and food were provided *ad libitum*. Female mice of 10–12 weeks of age were used. All experimental procedures were approved by the CTRI Institutional Animal Care and Use Committee (IACUC protocols #2, 7, 8, 11, approved on March 6, 2021). For adherence of macrophages to plastic, RPMI 1640 supplemented with 10% fetal calf serum (FCS), 10 mM HEPES, 2 mM L-glutamine, 1% nonessential amino acids, 1 mM pyruvate, $5x10^{-5}$ M 2-mercaptoethanol, and antibiotics (all components from HyClone, Carlington, The Netherlands) was used (medium 1). All assays were performed in a medium which differed from medium 1 in that it contained no antibiotics and only 2% FCS (medium 2) or 5% FCS (medium 3).

Lungs were enzymatically digested as described previously[76,77]. Briefly, blood vessels were washed out by heart perfusion with 0.02% EDTA-PBS through the right ventricle and cut vena cava, lungs removed, sliced into 1–2 mm^3 pieces, and incubated at 37°C for 90 min in supplemented RPMI-1640 containing 200 U/ml collagenase and 50 U/ml DNase-I (Sigma, MO). Single-cell suspensions were obtained by vigorous pipetting. The lung cells were washed twice in Hanks' balanced salt solution (HBSS) containing 2% FCS and antibiotics and resuspended in medium 1. Cells ($20x10^6$ to $30x10^6$) were incubated in 10 ml of medium 1 for 1.5 h on 90-mm-diameter treated Petri dishes (Costar-Corning, Badhoevedorp, The Netherlands) at 37°C, 5% CO_2. Nonadherent cells were removed by triple vigorous washing with warm antibiotic-free HBSS containing 2% FCS. Adherent cells were detached from the plastic by incubating the monolayers in 0.02% EDTA-PBS antibiotic-free solution for 30 min at room temperature. Cell suspensions were obtained by pipetting, washed twice with HBSS, and resuspended in medium 2.

Macrophage-mycobacteria co-culture

To obtain monolayers of good density, $5x10^4$ lung macrophages were plated in a well of a flat-bottom 96-well plate (Costar-Corning). Macrophages adhered for 1 h before live *M. tuberculosis* were added at the MOIs indicated in the figures and tables. After 14 h incubation, wells were gently washed to remove extracellular bacteria; then, warm medium 3 containing 1 mM ALA was added (200 µl per well). In 5 days of co-culture, $4x10^4$ of fresh macrophages were added to phagocyte extracellular bacteria released from

dying macrophages. After 11 days of total cultivation, the wells were washed from extracellular bacteria and *Mtb*-containing macrophages underwent illumination.

To test the possible bactericidal activity of porphyrins gained by macrophages during cultivation in the presence of ALA, we cultured lung macrophages in the presence or absence of 1 mM ALA for 10 days and then added 4-month-old dormant *Mtb* obtained in the presence or absence of ALA at MOI = 1. After 16 h of incubation, wells containing *M. tuberculosis* were gently washed to remove extracellular bacteria, and *Mtb*-containing macrophages underwent illumination.

Photos were taken using an AxioSkop40 microscope (Zeiss, Germany) and AX10 filter for porphyrins: BP 546/12 – FT 580 – LP 590.

Viability Evaluation by MPN

Most probable number (MPN) assays of *Mtb* were performed in 48-well plastic plates (Corning) containing 1 ml of special medium for the most effective reactivation of dormant *Mtb* cells[70]. The medium contained 3.25 g nutrient broth dissolved in 1 liter of a mixture of Sauton medium (0.5 g KH2PO4; 1.4 g $MgSO_4.7H_2O$; 4 g L-asparagine; 0.05 g ferric ammonium citrate; 2 g sodium citrate; 0.01% (w/v) $ZnSO_4.7H_2O$ per liter pH 7.0), Middlebrook 7H9 liquid medium (Himedia, India), and RPMI (Thermo Fisher Scientific, USA) (1:1:1) supplemented with 0.5% v/v glycerol, 0.05% v/v Tween 80, 10% ADC (Himedia, India). *Mtb* cells were serially 10-fold diluted in the reactivation medium. Appropriate five serial dilutions of *Mtb* cells (100 µl) were added to each well containing the same medium in triplicate. Plates were incubated at 37°C for 21 days. Wells with visible bacterial growth were counted as positive, and MPN values were calculated using standard statistical methods[78].

Isolation of RNA, Illumina sequencing

ALA was added to the cultures in a final concentration of 3 mM and the cultures were incubated for the next 2 h. Bacterial samples (active *M. tuberculosis* (MAC_1, MAC_2, MAC_3), dormant (DORM_1,DORM_2,DORM_3), active in the presence of 5-aminolevulinic acid (ALA) (MACALA_1,MACALA_2, MACALA_3), and also dormant in the presence of ALA (DORMALA_1, DORMALA_2, DORMALA_3) were chilled in triplicate on ice, harvested by centrifugation (4000 g, 15 min, 4°C), and 1 ml Trizol reagent was added to the pellets. Cells were disrupted using zirconia beads (0.1 mm) in a BeadBeater (Biospec, USA) with 100 µm zirconium beads, and centrifuged (4000g, 45 min, 4°C) to clear cell lysates from cell debris. After centrifugation, the supernatant was extracted once with chloroform. Nucleic acids were then precipitated with isopropanol, harvested by centrifugation, washed with 70% ethanol and re-dissolved in nuclease-free water (Promega, USA). RNA was then isolated using a RNeasy Mini kit (Qiagen). Each RNA sample was finally treated with RNase-free Turbo DNase (Life Technologies, Carlsbad, CA, USA) and purified with the RNeasy mini kit (Qiagen, Venlo, The Netherlands).

After RNA isolation, removal of excess ribosomal RNA as well as cDNA synthesis was performed using the Illumina TruSeq Stranded Total RNA With Illumina Ribo-Zero Plus rRNA Depletion kit (Illumina, San

Diego, CA, USA). The resulting cDNA was used to prepare libraries compatible with Illumina sequencing technology.

Processing of RNA-seq data

The quality of the resulting libraries was checked using the Fragment Analyzer. Quantitative analysis was performed by qPCR. After quality control and evaluation of the DNA quantity, the pool of libraries was sequenced on an Illumina NovaSeq 6000 instrument (length of reads —150 bp on both sides of the fragments). FASTQ files were generated using bcl2fastq Conversion Software v2.20 (Illumina, San Diego, CA, USA). As a result, 1,107,614,502 reads were received. The quality control of the sequencing results was carried out using the FastQC program (https://www.bioinformatics.babraham.ac.uk/projects/fastqc/). Reads were filtered and adapter sequences were removed using TrimGalore and Cutadapt (https://github.com/FelixKrueger/TrimGalore).

Sequencing analysis and mapping to M. tuberculosis H37Rv reference genome

After quality control evaluation and pruning of low-quality reads, the reads were mapped to the *M. tuberculosis* reference genome (https://www.ncbi.nlm.nih.gov/nuccore/NC_018143.2). Reads were mapped to the reference genome using HiSat2 [79]. The quality of the mapping results was assessed using RSeQC[80]. As a result of filtering out unsatisfactory reads, the percentage of reads mapped to the reference *M. tuberculosis* genome was ~ 97% of the total number of mapped reads. The expression level was calculated using HTSeq[81], and the subsequent bioinformatic analysis of ready-made expression matrices was carried out using DESeq2[82].

A table containing the data of the expression levels of all genes was added as Supplementary Materials Table S0. The Z-score was calculated from the mean and standard deviation of the reference dataset [83].

Photodynamic inactivation

Suspensions of dormant/active *Mtb* with OD = 0.1, which corresponds to ca. 10^7 bacteria per ml, were used for light inactivation experiments. Volumes of 100 µl were pipetted into the wells of a 96-well plate (Nunc). Illuminations of the samples were performed by LED SOLIS-4C (Thorlabs, USA) and interference filters with the band passes 565/24 nm (MF565-24, ThorLabs, USA) that correspond to the absorption peaks for both coproporphyrin and Zn-coproporphyrin (Fig. 4). Light power was measured by a Newport 2936-c power meter and was equal to 180 mW. Light beam was collimated to the diameter 6.5 mm that corresponded to the diameter of wells of a 96-well plate. Illumination coupling MT-CON (Thorlabs, USA) with optimized optics for bright bottom homogenous illumination of suspension in the wells was used. Illumination was for 5, 15, 30, or 60 min. Temperature control was performed by Fluke 80BK Type K Multimeter Thermocouple Temperature Probe directly in the microwell before and after illumination and in the presence of and without bacterial suspension with the precision ± 0.2°C.

Temperature was below 40°C in the wells during all the experiments.

After illumination of the samples, serial tenfold dilutions (10^{-1} to 10^{-7}) were prepared and bacterial viability was evaluated by MPN assay.

DCPIP Reduction

Endogenous respiration was determined by reduction in DCPIP (2,6-dichlorophenolindophenol) in the presence of menadione monitored spectrophotometrically at 600 nm. The reaction mixture (4 ml) contained 0.2 µmol 2,6-DCPIP, 0.6 µmol menadione, and 400 µl of the cell suspension in Sauton medium (pH 7.4).

Statistical analysis

Statistical processing was carried out via the analysis of the standard deviation or relative error within the data group. All the data are presented as the mean values of three replicate determinations. MPN values were determined using de Man's tables calculated on the basis of a Poisson distribution[78]. For the MPN assay, (95%) confidence limits were calculated. The MPN values were considered statistically different if low and high confidence limits were not overlapping.

The essentiality of statistics was determined at $p < 0.05$. The OriginPro software package 8.5 and Design Expert Software Version 8.0.6 were involved in the statistical analysis.

The corresponding p-values of comparison of the three groups of cells (dormant vs. active, dormant vs. dormant + ALA, active vs. active + ALA) in transcriptomic analysis were calculated from a two-sided t-test.

Declarations

Acknowledgements

The analysis (LC-MS and HR-MS) of porphyrins was carried out with the equipment of the Shared-Access Equipment Centre "Industrial Biotechnology" of Federal Research Center "Fundamentals of Biotechnology" Russian Academy of Sciences.

Author Contributions:

M.O.S., A.S.K. and A.P.S. conceptualization and wrote the main manuscript text;

M.O.S. prepared figure S1, S2, S5, S6, S7, S8 Table S3;

M.O.S. and A.P.S. antimicrobial PDT, prepared figure 1,6,8, Table S1;

I.A.L. and A.S.A. experiments with macrophage, prepared figure 7,8;

I.A.G. and A.P.S single cell and extract spectroscopy, prepared figure 2, 3, S3, S4;

M.O.S. and D.M.S. transcriptome, prepared figure 5;

G.N.V. and A.S.K. respiratory experiments, prepared Table 1;

A.M.T. HR-MS, prepared figure 4, Table S2.

All authors have read and agreed to the published version of the manuscript.

Funding

This study was funded by Russian Science Foundation grant 19-15-00324.

Transparency declarations

None to declare.

Ethical Statement.

Authors confirming the study is reported in accordance with ARRIVE guidelines (https://arriveguidelines.org). All experimental procedures were approved by the CTRI Institutional Animal Care and Use Committee (IACUC protocols #2, 7, 8, 11, approved on March 6, 2021)

Data availability.

The datasets generated and/or analysed during the current study are available in the ZENODO repository https://doi.org/10.5281/zenodo.8322146) or GEO SRA accession SRR26142264 (MAC_1), SRR26142263 (MAC_2), SRR26142260 (MAC_3), SRR26142259 (DORM_1), SRR26142258 (DORM_2), SRR26142257 (DORM_3), SRR26142256 (MACALA_1), SRR26142255 (MACALA_2), SRR26142254 (MACALA_3), SRR26142253 (DORMALA_1), SRR26142262 (DORMALA_2), SRR26142261 (DORMALA_3).

References

1. Patra, K., Batabyal, S., Mandal, K., Ghose, D. & Sarkar, J. Tuberculosis and COVID-19: A combined global threat to human civilization. *Clin. Epidemiol. Glob. Heal.* **15**, 101031 (2022).
2. Kaprelyants, A., Salina, E. & Makarov, V. How to Kill Dormant Mycobacterium Tuberculosis. *Int. J. Mycobacteriology* **7**, 399–400 (2018).
3. Feng, Y., Tonon, C. C., Ashraf, S. & Hasan, T. Photodynamic and antibiotic therapy in combination against bacterial infections : efficacy , determinants , mechanisms , and future perspectives. *Adv. Drug Deliv. Rev.* **177**, 113941 (2021).
4. Shleeva, M., Savitsky, A. & Kaprelyants, A. Photoinactivation of mycobacteria to combat infection diseases : current state and perspectives. *Appl Microbiol Biotechnol.* **105**, 4099–4109 (2021).
5. Hanakova, A. *et al.* The application of antimicrobial photodynamic therapy on S. aureus and E. coli using porphyrin photosensitizers bound to cyclodextrin. *Microbiol. Res.* **169**, 163–170 (2014).
6. Awad, M. M., Tovmasyan, A., Craik, J. D., Batinic-Haberle, I. & Benov, L. T. Important cellular targets for antimicrobial photodynamic therapy. *Appl. Microbiol. Biotechnol.* **100**, 7679–7688 (2016).

7. Skwor, T. A. *et al.* Photodynamic inactivation of methicillin-resistant Staphylococcus aureus and Escherichia coli: A metalloporphyrin comparison. *J. Photochem. Photobiol. B Biol.* **165**, 51–57 (2016).
8. Chen, L., Bai, H., Xu, J. F., Wang, S. & Zhang, X. Supramolecular Porphyrin Photosensitizers: Controllable Disguise and Photoinduced Activation of Antibacterial Behavior. *ACS Appl. Mater. Interfaces* **9**, 13950–13957 (2017).
9. Alenezi, K., Tovmasyan, A., Batinic-Haberle, I. & Benov, L. T. Optimizing Zn porphyrin-based photosensitizers for efficient antibacterial photodynamic therapy. *Photodiagnosis Photodyn. Ther.* **17**, 154–159 (2017).
10. Al-Mutairi, R., Tovmasyan, A., Batinic-Haberle, I. & Benov, L. Sublethal Photodynamic Treatment Does Not Lead to Development of Resistance. *Front. Microbiol.* **9**, 1–9 (2018).
11. Gyulkhandanyan, A. G. *et al.* Meso-substituted cationic 3-and 4-N-Pyridylporphyrins and their Zn(II) derivatives for antibacterial photodynamic therapy. *J. Innov. Opt. Health Sci.* **15**, 1–16 (2022).
12. Sadzuka, Y. *et al.* Study on liposomalization of zinc-coproporphyrin I as a novel drug in photodynamic therapy. *Int. J. Pharm.* **338**, 306–309 (2007).
13. Malik, Z., Ladan, H. & Nitzan, Y. Photodynamic inactivation of Gram-negative bacteria: problems and possible solutions. *J Photochem Photobiol B.* **14**, 262–266 (1992).
14. van der Meulen, F. W. *et al.* Photodynamic destruction of Haemophilus parainfluenzae by endogenously produced porphyrins. *J. Photochem. Photobiol. B Biol.* **40**, 204–208 (1997).
15. Nikitushkin, V. D. *et al.* The main pigment of the dormant Mycobacterium smegmatis is porphyrin. *FEMS Microbiol. Lett.* **363**, 1–8 (2016).
16. Shleeva, M. O. *et al.* Photoinactivation of dormant Mycobacterium smegmatis due to its endogenous porphyrins. *Appl. Microbiol. Biotechnol.* **103**, 9687–9695 (2019).
17. Shleeva, M. O., Savitsky, A. P., Nikitushkin, V. D., Soloviev, I. D. & Trutneva, K. A. Effect of Photodynamic Inactivation against Dormant Forms and Active Growing Cells of Mycobacterium smegmatis. *Appl. Biochem. Microbiol.* **56**, 242–249 (2020).
18. Shleeva, M. O. *et al.* Dormant ovoid cells of *Mycobacterium tuberculosis* are formed in response to gradual external acidification. *Tuberculosis* **91**, 146–154 (2011).
19. Shleeva, M. O. *et al.* Dormant ovoid cells of *Mycobacterium tuberculosis* are formed in response to gradual external acidification. *Tuberculosis* **91**, 146–154 (2011).
20. Shleeva, M. O. *et al.* Overexpression of Adenylyl Cyclase Encoded by the *Mycobacterium tuberculosis Rv2212* Gene Confers Improved Fitness, Accelerated Recovery from Dormancy and Enhanced Virulence in Mice. *Front. Cell. Infect. Microbiol.* **7**, 1–8 (2017).
21. Larralde, C. *et al.* Analysis of porphyrins and enzymes in porphyrin synthesis in Taenia solium cysticercus from man and pig. *Mol. Biochem. Parasitol.* **22**, 203–213 (1987).
22. Lukomsky, I., Gottfried, V. & Kimel, S. Delayed Fluorescence of Porphyrins in Different Media. *J. Fluoresc.* **4**, 49–51 (1994).

23. Falk, J. E. *Porphyrins and metalloporphyrins*. (1964).
24. Møller, J. K. S., Adamsen, C. E., Catharino, R. R., Skibsted, L. H. & Eberlin, M. N. Mass spectrometric evidence for a zinc – porphyrin complex as the red pigment in dry-cured Iberian and Parma ham. *Meat Sci.* **75**, 203–210 (2007).
25. Ignatov, D. V. *et al.* Dormant non-culturable Mycobacterium tuberculosis retains stable low-abundant mRNA. *BMC Genomics* **16**, 954 (2015).
26. Aanes, H. *et al.* Normalization of RNA-sequencing data from samples with varying mRNA levels. *PLoS One* **9**, 1–7 (2014).
27. Layer, G. Heme biosynthesis in prokaryotes. *BBA - Mol. Cell Res.* **1868**, 118861 (2021).
28. Xiong, Y., Chalmers, M. J., Gao, F. P., Cross, T. A. & Marshall, A. G. Identification of Mycobacterium tuberculosis H37Rv integral membrane proteins by one-dimensional gel electrophoresis and liquid chromatography electrospray ionization tandem mass spectrometry. *J. Proteome Res.* **4**, 855–861 (2005).
29. Målen, H., Pathak, S., Søfteland, T., de Souza, G. A. & Wiker, H. G. Definition of novel cell envelope associated proteins in Triton X-114 extracts of Mycobacterium tuberculosis H37Rv. *BMC Microbiol.* **10**, 132 (2010).
30. Petrovieh, R. M., Litwin, S. & Jaffe, E. K. Bradyrhizobium japonicum porphobilinogen synthase uses two Mg(II) and monovalent cations. *J. Biol. Chem.* **271**, 8692–8699 (1996).
31. Golby, P. *et al.* Characterization of two in vivo-expressesd methyltransferases of the Mycobacterium tuberculosis complex: Antigenicity and genetic regulation. *Microbiology* **154**, 1059–1067 (2008).
32. Biketov, S. *et al.* Culturability of Mycobacterium tuberculosis cells isolated from murine macrophages: A bacterial growth factor promotes recovery. *FEMS Immunol. Med. Microbiol.* **29**, 233–240 (2000).
33. Azarkina, N. & Konstantinov, A. A. Stimulation of menaquinone-dependent electron transfer in the respiratory chain of Bacillus subtilis by membrane energization. *J. Bacteriol.* **184**, 5339–5347 (2002).
34. Lukoianova, M. & Koroleva, V. Menaquinone function in the respiratory chain of Micrococcus lysodeikticus. *Biokhimiia* **40**, 1154–62 (1975).
35. Shuvalov, V. & Krasnovskii, A. The luminescence of zinc-porphyrins in microorganisms and plants: phosphorescence and delayed fluorescence. *Mol Biol.* **5**, 557–66 (1971).
36. Petukhov, V. & Osin, N. Phosphorimetric method to determine Zn- porphyrins in microorganisms and biological liquids. *Prikl Biokhim Mikrobiol.* **16**, 284–90 (1980).
37. Plus, R. A Review of In Vivo Studies of Porphyrins and Unexpected Fluorescences. An Interpretation of the Results. *Med. Hypotheses* **37**, 49–57 (1992).
38. Koenig, K. & Schneckenburger, H. Laser-Induced Autofluorescence for Medical Diagnosis. *J. Fluoresc.* **4**, 17–40 (1994).

39. Ohsaki, Y. *et al.* Observation of Zn-photoprotoporphyrin red Autofluorescence in human bronchial cancer using color-fluorescence endoscopy. *BMC Cancer* **17**, 1–7 (2017).
40. Horiuchi, K. *et al.* Isolation and characterization of zinc coproporphyrin I: A major fluorescent component in meconium. *Clin. Chem.* **37**, 1173–1177 (1991).
41. Kilercik, M. *et al.* Zinc protoporphyrin levels in COVID-19 are indicative of iron deficiency and potential predictor of disease severity. *PLoS One* **17**, e0262487 (2022).
42. Labbe, R. F., Vreman, H. J. & Stevenson, D. K. Zinc Protoporphyrin: A Metabolite with a Mission. *Clin. Chem.* **45**, 2060–2072 (1999).
43. Bhuiyan, M. N. I. *et al.* Zincmethylphyrins and coproporphyrins, novel growth factors released by Sphingopyxis sp., enable laboratory cultivation of previously uncultured Leucobacter sp. through interspecies mutualism. *J. Antibiot. (Tokyo).* **69**, 97–103 (2016).
44. Dailey, T. A. *et al.* Discovery and Characterization of HemQ. *J. Biol. Chem.* **285**, 25978–25986 (2010).
45. Dailey, H. A., Gerdes, S., Dailey, T. A., Burch, J. S. & Phillips, J. D. Noncanonical coproporphyrin-dependent bacterial heme biosynthesis pathway that does not use protoporphyrin. *Proc. Natl. Acad. Sci. U. S. A.* **112**, 2210–2215 (2015).
46. Shleeva, M., Savitsky, A. & Kaprelyants, A. Corynebacterium jeikeium Dormant Cell Formation and Photodynamic Inactivation. *Front. Microbiol.* **11**, 605899 (2020).
47. Berney, M. & Cook, G. M. Unique flexibility in energy metabolism allows mycobacteria to combat starvation and hypoxia. *PLoS One* **5**, (2010).
48. Albrethsen, J. *et al.* Proteomic Profiling of *Mycobacterium tuberculosis* identifies nutrient-starvation-responsive toxin–antitoxin systems. *Mol. Cell. Proteomics* **12**, 1180–1191 (2013).
49. Yatsimirsky, A. K., Nelen, M. I., Savitsky, A. P. & Ponamarev, G. V. Kinetic fluorimetric determination of Cu(II) and Zn(II) by their incorporation reactions into a water-soluble porphyrin. *Talanta* **41**, 1699–1706 (1994).
50. Takemura, T., Ohta, N., Nakajima, S. & Sakata, I. Critical Importance of the Triplet Lifetime of Photosensitizer in Photodynamic Therapy of Tumor. *Photochem. Photobiol.* **50**, 339–344 (1989).
51. Liu, Y., Qin, R., Zaat, S. A. J., Breukink, E. & Heger, M. Antibacterial photodynamic therapy: overview of a promising approach to fight antibiotic-resistant bacterial infections. *J. Clin. Transl. Res.* **1**, 140–167 (2015).
52. Sung, N. *et al.* Inactivation of multidrug resistant (MDR)- and extensively drug resistant (XDR)-Mycobacterium tuberculosis by photodynamic therapy. *Photodiagnosis Photodyn. Ther.* **10**, 694–702 (2013).
53. Shih, M. H. & Huang, F. C. Effects of photodynamic therapy on rapidly growing nontuberculous mycobacteria keratitis. *Investig. Ophthalmol. Vis. Sci.* **52**, 223–229 (2011).
54. O'Riordan, K. *et al.* Photoinactivation of mycobacteria in vitro and in a new murine model of localized Mycobacterium bovis BCG-induced granulomatous infection. *Antimicrob. Agents Chemother.* **50**, 1828–1834 (2006).

55. Wiegell, S. R., Kongshoj, B. & Wulf, H. C. Mycobacterium marinum infection cured by photodynamic therapy. *Arch. Dermatol.* **142**, 1241–1242 (2006).
56. Feese, E. & Ghiladi, R. A. Highly efficient in vitro photodynamic inactivation of Mycobacterium smegmatis. *J. Antimicrob. Chemother.* **64**, 782–785 (2009).
57. Dirschka, T. *et al.* Long-term (6 and 12 months) follow-up of two prospective, randomized, controlled phase III trials of photodynamic therapy with BF- 200 ALA and methyl aminolaevulinate for the treatment of actinic keratosis. *Br. J. Dermatol.* **168**, 825–836 (2013).
58. Reinhold, U. A review of BF-200 ALA for the photodynamic treatment of mild-to-moderate actinic keratosis. *Futur. Oncol.* **13**, 2413–2428 (2017).
59. Petrini, M. *et al.* Photodynamic Antibiofilm and Antibacterial Activity of a New Gel with 5-Aminolevulinic Acid on Infected Titanium Surfaces. *Biomedicines* **10**, 572 (2022).
60. Wang, X. *et al.* ALA_PDT Promotes Ferroptosis-Like Death of Mycobacterium abscessus and Antibiotic Sterilization via Oxidative Stress. *Antioxidants* **11**, 546 (2022).
61. Yue, C. *et al.* In vitro study of the effect of ALA-PDT on Mycobacterium abscessus and its antibiotic susceptibility. *Photodiagnosis Photodyn. Ther.* **38**, 102802 (2022).
62. Sun, K. *et al.* A new approach to the treatment of nontuberculous mycobacterium skin infections caused by iatrogenic manipulation: Photodynamic therapy combined with antibiotics: A pilot study. *Photodiagnosis Photodyn. Ther.* **37**, 102695 (2022).
63. Zhang, Z. *et al.* Successful treatment of tuberculosis verrucosa cutis with fester as primary manifestation with photodynamic therapy and anti-tubercular drugs. *Photodiagnosis Photodyn. Ther.* **38**, 102763 (2022).
64. Ozog, D. M. *et al.* Photodynamic Therapy : A Clinical Consensus Guide. *Dermatol Surg Off Publ Am Soc Dermatol Surg* **42**, 804–827 (2016).
65. Li, X., Lovell, J. F., Yoon, J. & Chen, X. Clinical development and potential of photothermal and photodynamic therapies for cancer. *Nat. Rev. Clin. Oncol.* **17**, 657–74 (2020).
66. Zhou, X. *et al.* Architecture of the mycobacterial succinate dehydrogenase with a membrane-embedded rieske FeS cluster. *Proc. Natl. Acad. Sci. U. S. A.* **118**, e2022308118 (2021).
67. Lennicke, C. & Cochemé, H. M. Redox metabolism: ROS as specific molecular regulators of cell signaling and function. *Mol. Cell* **81**, 3691–3707 (2021).
68. Cabiscol, E., Tamarit, J. & Ros, J. Oxidative stress in bacteria and protein damage by reactive oxygen species. *Int Microbiol* **3**, 3–8 (2000).
69. Li, X., Lovell, J. F., Yoon, J. & Chen, X. Clinical development and potential of photothermal and photodynamic therapies for cancer. *Nat. Rev. Clin. Oncol.* **17**, 657–74 (2020).
70. Trutneva, K. A., Shleeva, M. O., Demina, G. R., Vostroknutova, G. N. & Kaprelyans, A. S. One-Year Old Dormant, “Non-culturable” Mycobacterium tuberculosis Preserves Significantly Diverse Protein Profile. *Front. Cell. Infect. Microbiol.* **10**, 1–12 (2020).

71. Bligh, E. . & Dyer, W. J. A rapid method of total lipid extraction and purification. *Can. J. Biochem. Physiol.* **37**, 911–917 (1959).
72. Mantrova, E. Y., Demcheva, M. V. & Savitsky, A. P. Universal phosphorescence immunoassay. *Anal. Biochem.* **219**, 109–114 (1994).
73. Hocking, R. R. *Methods and Applications of Linear Models. Regression and Analysis of Variance. Chapter 3, Transforming the Data, 3.2 Weighted least squares*. (Wiley Series in Probability and Statistics, 2013). doi:10.1002/0471434159
74. Nocedal, J. & Wright, S. J. *Numerical Optimization. Chapter 10, Least-Squares Problems, Methods for large-residual problems*. (Springer, 2006).
75. Baek, S.-J., Park, A., Ahn, Y.-J. & Choo, J. Baseline correction using asymmetrically reweighted penalized least squares smoothing. *Analyst* **140**, 250–257 (2015).
76. Apt, A. S. *et al.* Distinct H-2 complex control of mortality , and immune responses to tuberculosis infection in virgin and BCG-vaccinated mice. *Clin Exp Immunol* **94**, 322–329 (1993).
77. Eruslanov, E. B. *et al.* Lung cell responses to M. tuberculosis in genetically susceptible and resistant mice following intratracheal challenge. *Clin. Exp. Immunol.* **135**, 19–28 (2004).
78. de Man, J. C. The probability of most probable numbers. *Eur. J. Appl. Microbiol.* **1**, 67–78 (1974).
79. Kim, D., Langmead, B. & Salzberg1, S. L. HISAT: a fast spliced aligner with low memory requirements. *Nat. Methods* **12**, 357–360 (2015).
80. Wang, L., Wang, S. & Li, W. RSeQC: Quality control of RNA-seq experiments. *Bioinformatics* **28**, 2184–2185 (2012).
81. Anders, S., Pyl, P. T. & Huber, W. HTSeq-A Python framework to work with high-throughput sequencing data. *Bioinformatics* **31**, 166–169 (2015).
82. Love, M. I., Huber, W. & Anders, S. Moderated estimation of fold change and dispersion for RNA-seq data with DESeq2. *Genome Biol.* **15**, 550 (2014).
83. Ben Salah, N. *et al.* The Z-score: a new tool in the interpretation of spirometric data. *Tunis Med.* **95**, 767–771 (2017).

Figures

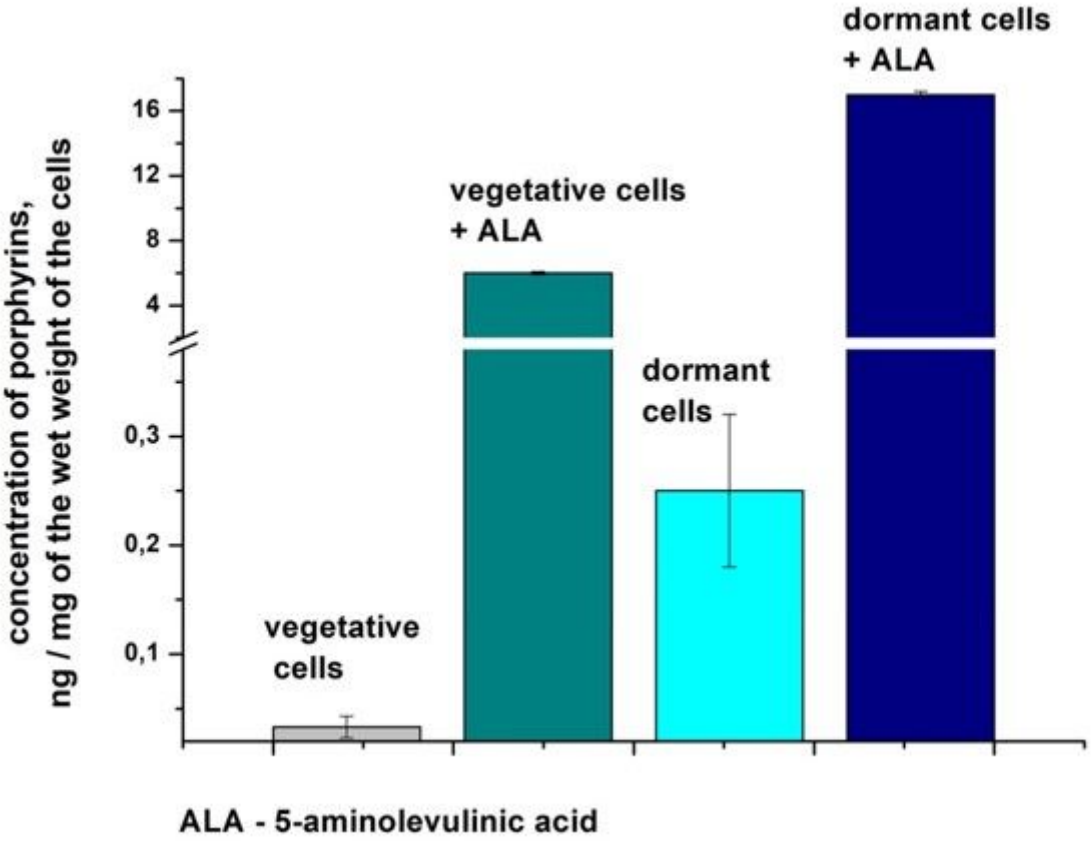

Figure 1

5-aminolevulenic acid (ALA) stimulates the synthesis of endogenous porphyrins in *M. tuberculosis.* Vegetative cells of *M. tuberculosis* cells were grown in Middlebrook 7H9 liquid medium supplemented with ADC and Tween-80 for 10 d (initial bacteria concentration 10^5 cells per ml). After 3 days post inoculation 3 mM ALA was added to some flasks. Dormant *Mtb* cells were obtained in modified Sauton's medium as described in M&M. ALA (3 mM) was added after 20 d post inoculation. F acidification in the stationary growth phase and an earlier formation of dormant forms (Figure S1). However, without illumination this deviation from the usual rate of formation of dormant mycobacteria did not affect the ability of cells to reactivate judged by MPN assay. Moreover, "+ALA" cells after a long-team period of dormancy (up to 3 years) preserved their potential viability for a longer time in comparison with dormant cells obtained under standard conditions (Figure S2). Thus, ALA itself does not influence the formation of dormant *Mtb* cells.

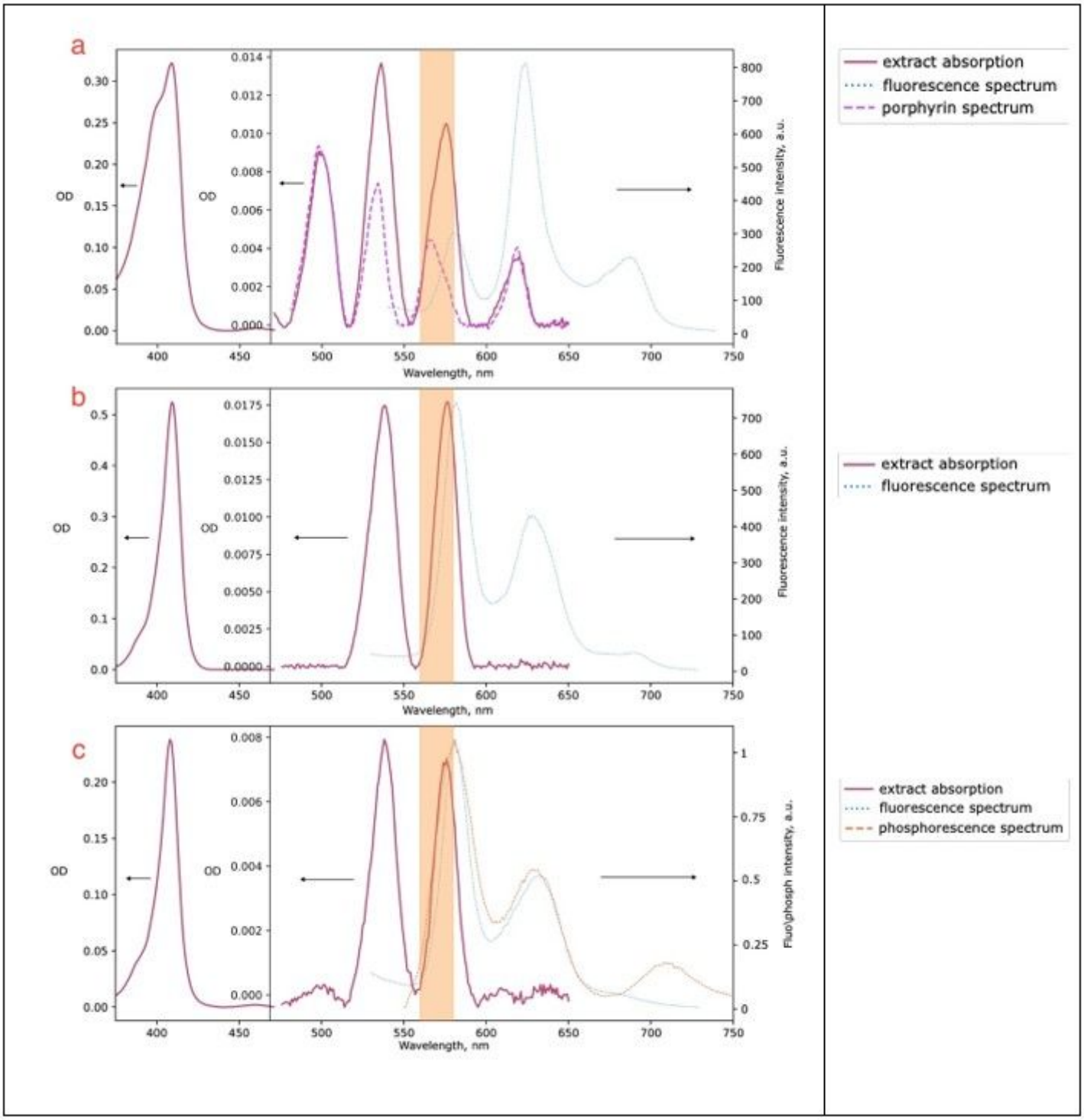

Figure 2

Spectra of the extracts of vegetative and dormant *M. tuberculosis* cells grown in the presence of ALA. *Mtb* cells were inoculated in Middlebrook 7H9 liquid medium supplemented by ADC, Tween-80, and 3 mM ALA at a concentration of 10^5 cells per ml, followed by incubation at 37 °C, under agitation of 200 rpm. After 20 d, biomass was collected by centrifugation and successively extracted with chloroform-methanol-water and then with 2% Triton x 100 (for details see the M&M section). Dormant *Mtb* cells were obtained as described in the M&M section. Then, 3 mM of ALA was added after 20 d post inoculation.

Sixty-day-old dormant mycobacteria were harvested and porphyrins were extracted. The orange area corresponds to the illumination at 565/24 nm. A) Absorption and fluorescence spectra chloroform-methanol-water extract of vegetative *Mtb* cells grown in the presence of ALA. Mostly free porphyrin was extracted with a certain amount of Zn porphyrin. B) Absorption and fluorescence spectra at 410 nm excitation of 2% Triton X-100 extract of vegetative *Mtb* cells grown in the presence of ALA. Preferential extraction of Zn porphyrin with a small admixture of free porphyrin. C) Absorption, fluorescence, and phosphorescence spectra at 410 nm excitation of 2% Triton x100 extract of dormant *Mtb* cells grown in the presence of ALA. Preferential extraction of Zn porphyrin with a small admixture of free porphyrin.

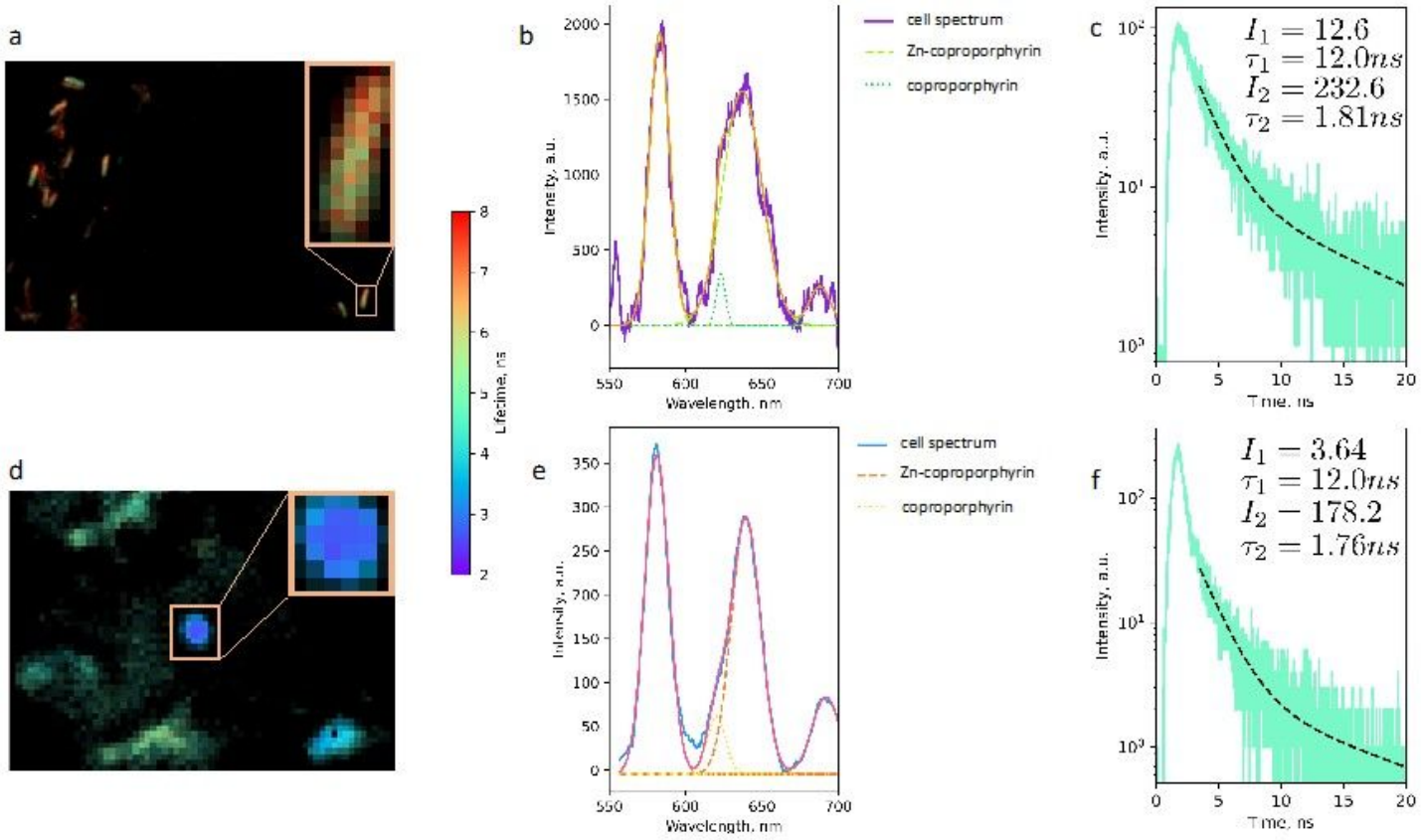

Figure 3

Single mycobacterial cell fluorescence emission spectra for both vegetative and dormant cells of mycobacterial cell obtained with laser scanning confocal microscopy. Vegetative cells of *M. tuberculosis* cells were grown in Middlebrook 7H9 liquid medium supplemented by ADC and Tween-80 for 10 d (initial bacteria concentration 10^5 cells per ml). After 3 days post inoculation 3 mM ALA was added to some flasks. Dormant *Mtb* cells were obtained in modified Sauton's medium as described in M&M. ALA (3 mM) was added after 20 d post inoculation. Next, 20-day-old vegetative cells and 60-day-old dormant cells were applied to a glass cover slip and left to dry for a few minutes. Remaining cells were fixated with Merckoglass (Merck). After evaporation of solvent, samples were used for microscopy. Fluorescence spectra of coproporphyrin from bacteria stained in Merkoglas. Excitation by 405 nm laser with 550 nm

Long-pass emission filter. Confocal mode of measurements. Life-time images for vegetative cells (A) and for dormant cells (D). Fluorescence spectra of porphyrin from single vegetative (B) and dormant bacteria (E). Life-time decay for vegetative (C) and dormant (F) cells.

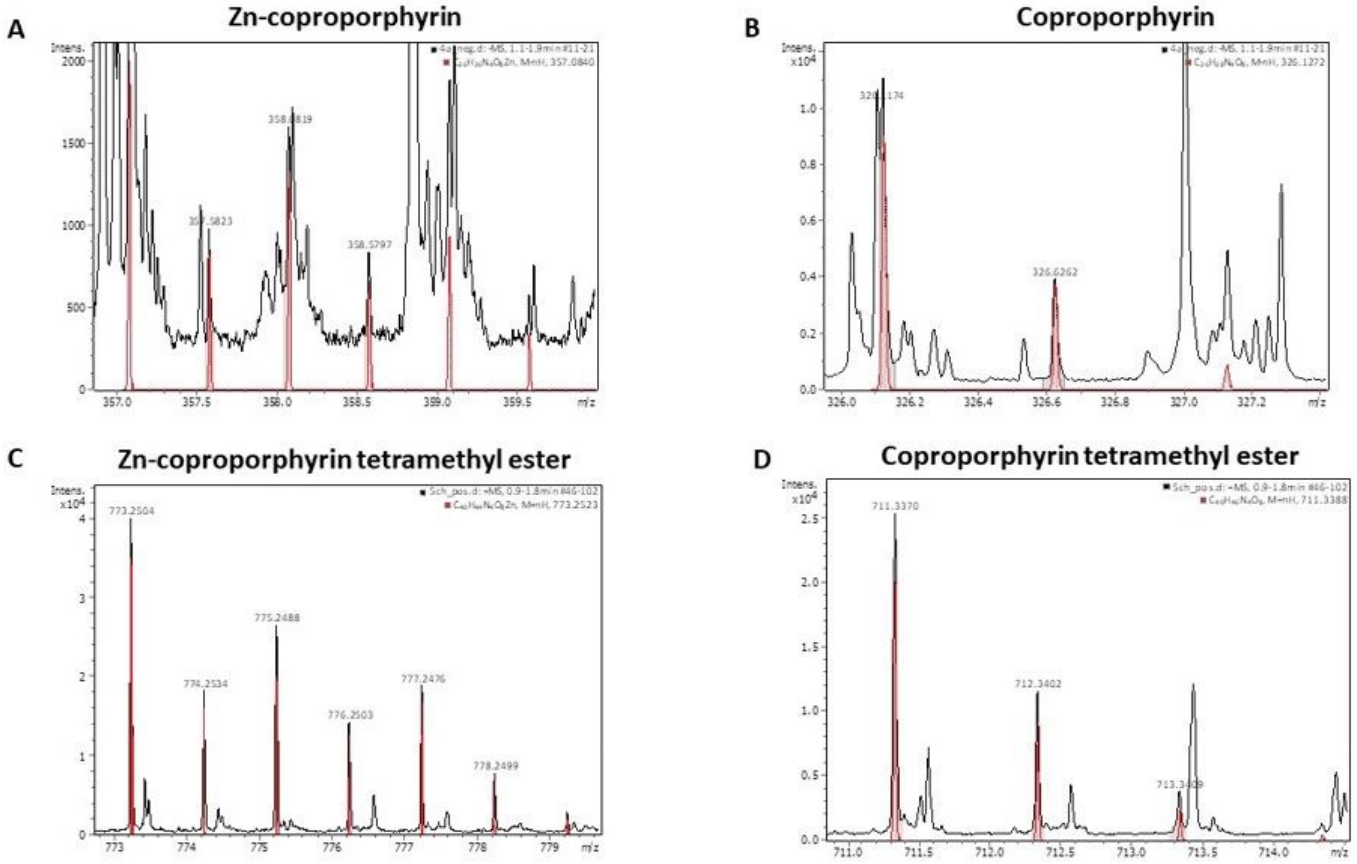

Figure 4

HR-MS spectra in the negative ion mode of extracts of vegetative *M. tuberculosis* cells (a, b) and in the positive ion mode of extracts of dormant mycobacteria (c, d) in 75% acetone:15% methanol:10% water solution showing a characteristic isotopologue distribution of Zn–porphyrin complexes.

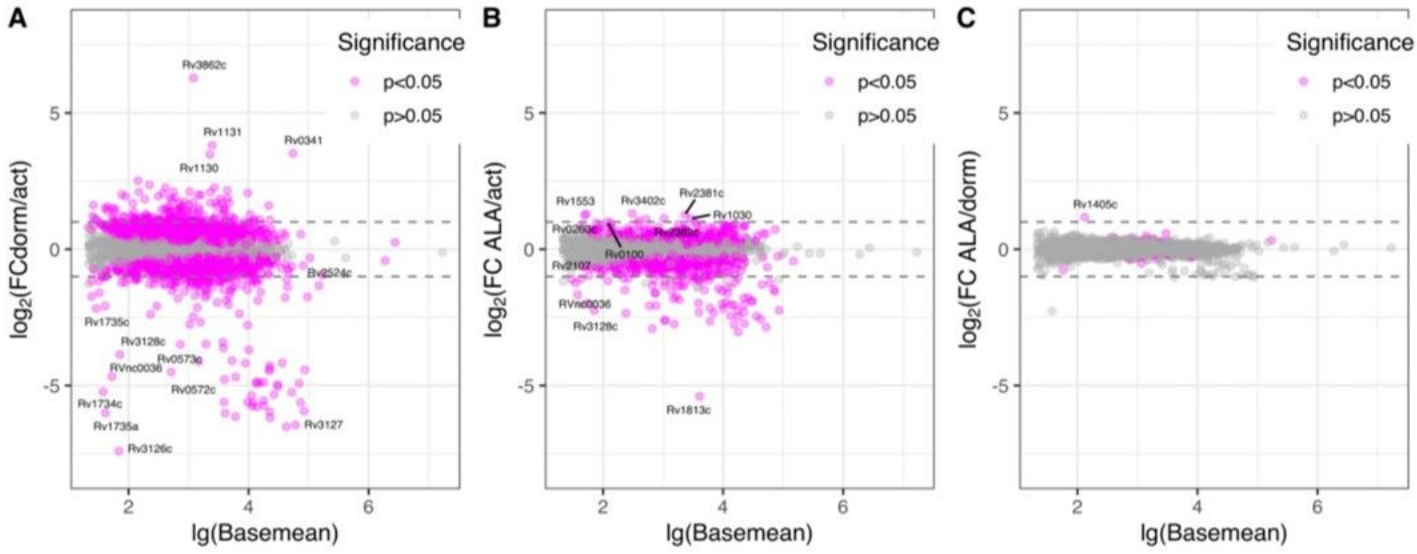

Figure 5

Dependence of the change in the ratio of the level of gene expression in the comparison groups on the normalized average level of *M. tuberculosis* gene expression. The statistical significance of the changes (p value) was calculated based on the Wald statistic. Since multiple comparisons of experimental groups were used, the final value of p was calculated taking into account the Benjamini-Hochberg correction.

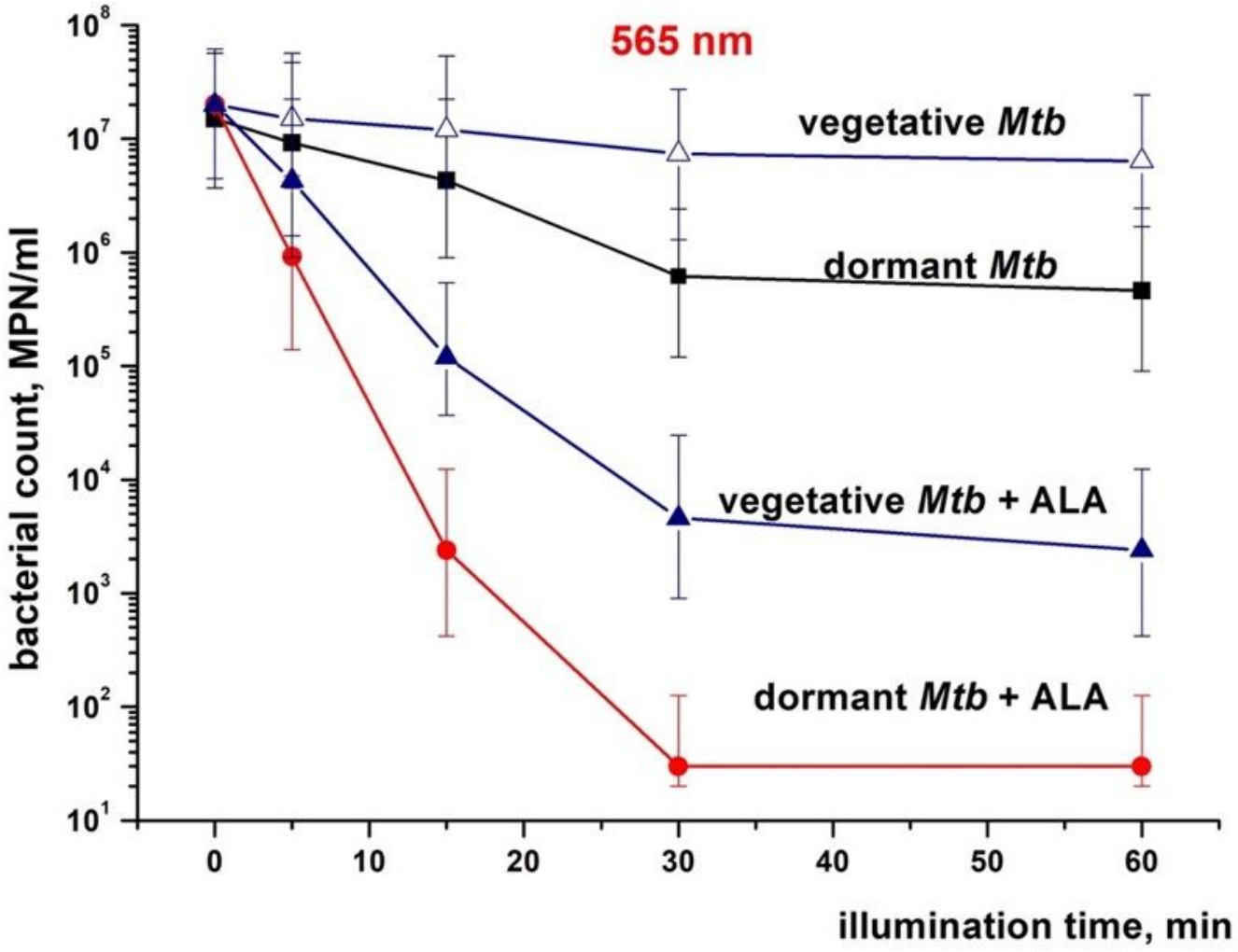

Figure 6

Photodynamic inactivation *M. tuberculosis* cells by light illumination at 565 nm. Dormant and vegetative *Mtb*cells were subjected to PDI as described in M&M, at a different time of illumination at 565/24 nm (corresponding to the orange area in Figure 4), under static conditions. After exposure, cell viability was estimated by MPN assay. Open triangles - vegetative *Mtb*, closed squares – dormant *Mtb,* closed triangles – vegetative *Mtb* grown in the presence of 3 mM ALA, closed circles – dormant *Mtb* obtained in the presence of 3 mM ALA.

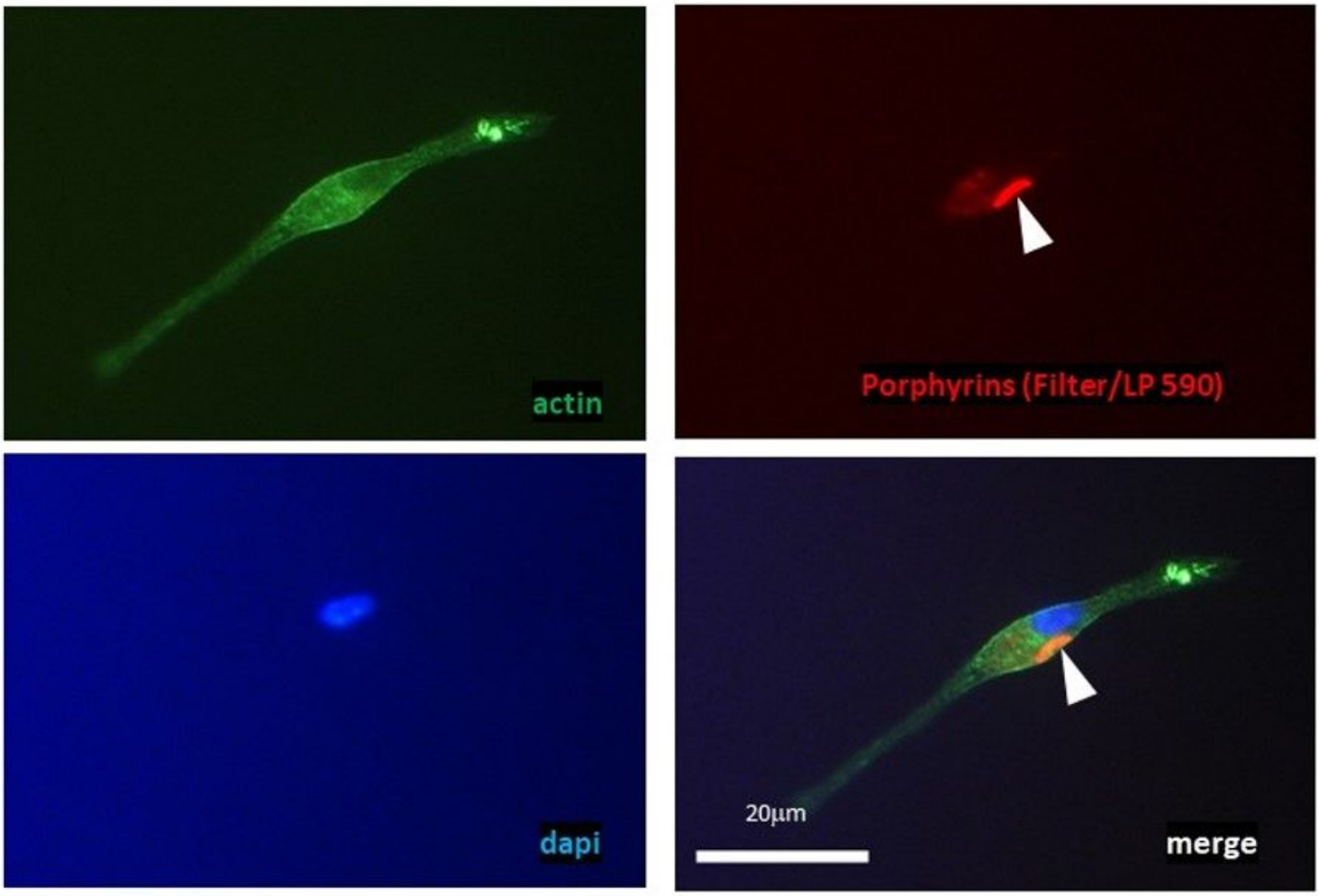

Figure 7

Macrophage containing porphyrin-rich vegetative *M. tuberculosis* cell grown in presence of ALA. Vegetative *Mtb* cells can produce and accumulate porphyrins within 10 days of co-culture with lung macrophages in the presence of 1 mM ALA. In mycobacteria captured by macrophages, fluorescence characteristic of porphyrins was observed. Visualization of red-fluorescent mycobacteria (filter Lp590) within lung macrophage, counerstained with ActinGreen and DAPI (blue). The white arrow points to the mycobacteria inside the macrophage.

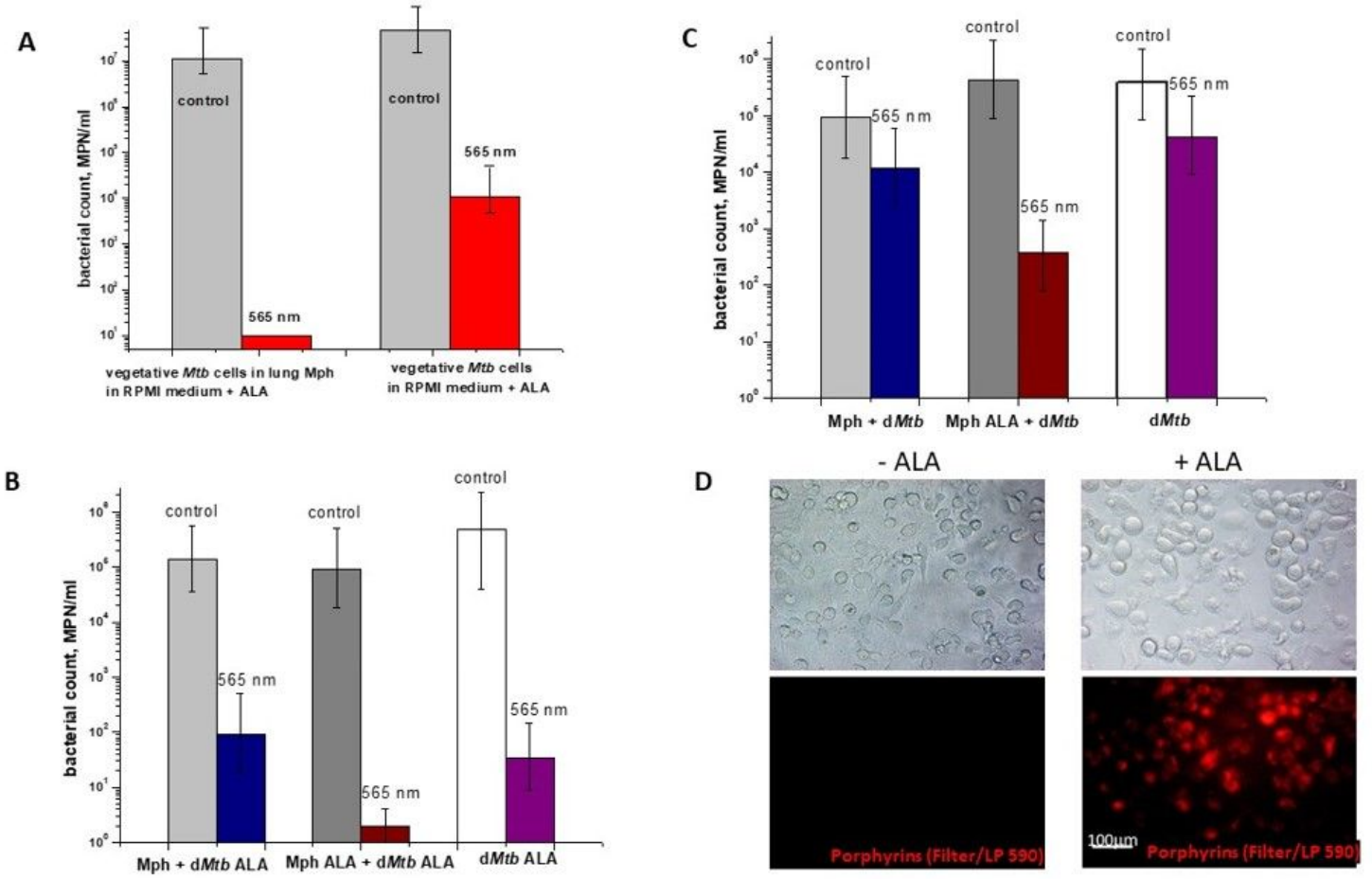

Figure 8

Photodynamic inactivation of vegetative *M. tuberculosis* cells (A) **and dormant *M. tuberculosis* cells** (B, C) **captured by lung macrophages.**

A) After 10 days of co-culture vegetative mycobacteria with lung macrophages in the presence of 3 mM ALA.

B) Macrophages and dormant mycobacteria were grown separately. Dormant mycobacteria were obtained in the presence of 3 mM ALA. Macrophages were obtained in the presence and absence of 3 mM ALA. The bacteria were then captured by macrophages as described in the M&M section.

C) Macrophages and dormant mycobacteria were grown separately. Dormant mycobacteria were obtained in the absence of ALA. Macrophages were obtained in the presence and absence of 1 mM ALA. The bacteria were then captured by macrophages as described in the M&M section.

D) Fluorescence microscopy of macrophages grown in the presence and absence of ALA. Images were performed by invert fluorescent microscope Axio Observer.A1 (Zeiss, Germany), AxioCam MRc5, filter for porphyrins: BP 546/12 – FT 580 – LP 590.

Supplementary Files

This is a list of supplementary files associated with this preprint. Click to download.

- supplementary1.docx